Rotating a Supersolid Dipolar Gas

S. M. Roccuzzo, A. Gallemí, A. Recati,* and S. Stringari
INO-CNR BEC Center and Dipartimento di Fisica, Università degli Studi di Trento, 38123 Povo, Italy
and Trento Institute for Fundamental Physics and Applications, INFN, 38123 Trento, Italy

(Received 18 October 2019; published 31 January 2020)

Distinctive features of supersolids show up in their rotational properties. We calculate the moment of inertia of a harmonically trapped dipolar Bose-Einstein condensed gas as a function of the tunable scattering length parameter, providing the transition from the (fully) superfluid to the supersolid phase and eventually to an incoherent crystal of self-bound droplets. The transition from the superfluid to the supersolid phase is characterized by a jump in the moment of inertia, revealing its first order nature. In the case of elongated trapping in the plane of rotation, we show that the moment of inertia determines the value of the frequency of the scissors mode, which is significantly affected by the reduction of superfluidity in the supersolid phase. The case of an in-plane isotropic trapping is instead well suited to study the formation of quantized vortices, which are shown to be characterized, in the supersolid phase, by a sizeable deformed core, caused by the presence of the surrounding density peaks.

DOI: 10.1103/PhysRevLett.124.045702

The study of the rotational behavior of a many-body system provides a crucial test to identify the effects of superfluidity. This test became particularly important when experimentalists tried to investigate the possible signature of superfluidity in a crystal of solid ^{4}He [1], looking for deviations of the moment of inertia from the classical rigid body value by means of a torsional oscillator. These experiments were later shown to be inconclusive in providing evidence for the long sought effect of supersolidity [2,3]. Ultracold atoms have eventually proved to be more efficient platforms. In 2017, two experiments reported on the first creation of supersolidity employing Bose-Einstein condensates inside optical resonators [4,5] and spin-orbit coupled mixtures [6]. The teams of Florence [7], Stuttgart [8], and Innsbruck [9] later observed supersolid properties in a harmonically trapped dipolar Bose-Einstein condensate, revealing at the same time the effects of the crystal modulation of the density profiles and the ones of coherence. More recent works of the same teams [10–12] measured the Goldstone modes associated with the spontaneous breaking of the relevant symmetries characterizing the supersolid phase. On the theoretical side, much work has been devoted in the past to the description of the supersolid phase of many-body systems and their superfluid behavior [13–17], emphasizing the peculiar features exploited by systems interacting with soft-core finite-range potentials [18–21], the role of spin-orbit coupling [22] and of long-range dipolar interactions [23–26].

The purpose of the present Letter is to provide first theoretical predictions concerning the rotational properties of a harmonically trapped supersolid dipolar gas, yielding unique information on the superfluid behavior of such a system, through the deviation of its moment of inertia from the rigid value and the emergence of quantized vortices. Special emphasis will be given to the role played by the trapping potential which favors the direct observability of these relevant superfluid effects. The moment of inertia characterizes the global superfluid behavior of the nonuniform system and can be easily calculated also in the presence of harmonic trapping and inhomogeneous configurations. In the presence of elongated trapping in the plane of rotation, the moment of inertia dictates the value of the experimentally measurable frequency of the scissors mode, corresponding to an oscillating rotation of the gas. Isotropic trapping is instead well suited to host quantized vortices. These are predicted to exhibit a peculiar deformed core of large size, due to the strong reduction of the density in the interstitial region surrounding the high density peaks, which characterize the supersolid phase. Interestingly, in the incoherent droplets state, we always find a finite nonclassical rotational inertia, due to the single droplet superfluidity.

Moment of inertia and the scissors mode.—The scissors mode [27,28] was first observed in nuclear physics [29], where it consists of the relative oscillating rotation between neutrons and protons in deformed atomic nuclei. In atomic physics, it was predicted [30] and soon measured [31] in atomic Bose-Einstein condensates confined by an anisotropic external potential, confirming the typical irrotational behavior predicted by superfluidity. It was later studied and observed also in ultracold Fermi gases [32,33] and in two-dimensional (2D) Bose gases [34] as well as, more recently, in droplets of dipolar gases [35]. An easy estimate of the frequency of the scissors mode is provided by the sum rule approach [36] based on the ratio $(\hbar\omega_{\rm sc})^2 = m_1(L_z)/m_{-1}(L_z)$ between the energy weighted and the

inverse energy weighted moments $m_p(L_z) = \int d\omega \omega^p S(L_z,\omega)$ of the dynamic structure factor $S(L_z,\omega) = \sum_n |\langle n|\hat{L}_z|0\rangle|^2 \delta(\hbar\omega - \hbar\omega_n)$ relative to the angular momentum operator $\hat{L}_z$. Assuming the gas is confined in a harmonic potential $V_{\rm ho}(\mathbf{r}) = m/2(\omega_x^2 x^2 + \omega_y^2 y^2 + \omega_z^2 z^2)$, the energy weighted moment takes the form (f-sum rule) $2m_1(L_z) = \langle[\hat{L}_z,[\hat{H},\hat{L}_z]]\rangle = N\hbar^2 m(\omega_y^2 - \omega_x^2)\langle x^2 - y^2\rangle$, with N and m the atom number and the atom mass, respectively. It holds in general for central potentials commuting with the angular momentum operator, and hence applies also to the case of the anisotropic dipolar interaction, provided one chooses the component of the angular momentum along the direction (z) of the dipole moments. In this case, the commutator $[\sum_{ij} V_{dd}(\mathbf{r}_i - \mathbf{r}_j), \hat{L}_z]$ vanishes identically, $V_{dd}(\mathbf{r}_i - \mathbf{r}_j) = (\mu_0\mu^2/4\pi)[(1-3\cos^2\theta)/(|\mathbf{r}_i - \mathbf{r}_j|^3)]$ being the dipole-dipole interaction between two identical magnetic dipoles aligned along the z axis, θ the angle between the vector $\mathbf{r}_i - \mathbf{r}_j$ and the polarization direction z, while μ is the atomic dipole moment and μ_0 the vacuum permeability. The inverse energy weighted moment is instead related to the moment of inertia per particle Θ through the relation $2m_{-1}(L_z) = N\Theta$. It can be calculated by applying the static perturbation $-\Omega\hat{L}_z$ to the system and using the standard definition $N\Theta = \lim_{\Omega\to 0}\langle\hat{L}_z\rangle/\Omega$. Thus, the frequency of the scissors mode takes the useful expression

$$(\hbar\omega_{\rm sc})^2 = \frac{\hbar^2 m(\omega_y^2 - \omega_x^2)\langle x^2 - y^2\rangle}{\Theta}. \tag{1}$$

At zero temperature, the dipolar gas is characterized by a macroscopic wave function $\Psi(\mathbf{r},t)$ that obeys the extended Gross-Pitaevskii equation (eGPE) [37]

$$i\frac{\partial}{\partial t}\Psi(\mathbf{r},t) = \Big[-\frac{\hbar^2}{2m}\nabla^2 + V_{\rm ho}(\mathbf{r}) + g|\Psi(\mathbf{r},t)|^2 + \int d\mathbf{r}' V_{dd}(\mathbf{r}-\mathbf{r}')|\Psi(\mathbf{r}',t)|^2 + \gamma(\varepsilon_{dd})|\Psi(\mathbf{r},t)|^3\Big]\Psi(\mathbf{r},t), \tag{2}$$

where the coupling constant $g = 4\pi\hbar^2 a/m$ is fixed by the s-wave scattering length a and $\varepsilon_{dd} = \mu_0\mu^2/(3g) = a_{dd}/a$ (a_{dd} is the so-called dipolar length) is the ratio between the strength of the dipole-dipole and the contact interaction. The last term is the local density approximation of the beyond-mean-field Lee-Huang-Yang (LHY) correction [38,39], with $\gamma(\varepsilon_{dd}) = (16/3\sqrt{\pi})ga^{\frac{3}{2}}\int_0^\pi d\theta \sin\theta[1+\varepsilon_{dd}(3\cos^2\theta - 1)]^{\frac{5}{2}}$. The LHY term is crucial in order to describe the supersolid phase and the occurrence of self-bound droplets. The use of the LHY term in Eq. (2) has been shown to work pretty well when compared with more microscopic (Monte Carlo) calculations [40] and to properly capture the physics of the system when compared with experiments. The same has been shown to be the case for self-bound droplets of quantum mixtures [41–45].

First of all, we determine the ground state configurations by evolving the eGPE in imaginary time starting from a guess wave function. For the sake of concreteness, we consider $N = 4\times10^4$ ^{164}Dy atoms confined in a harmonic potential with trapping frequencies equal to $\omega_{x,y,z} = 2\pi\times(20,40,80)$ Hz. Such isotope has a dipolar length $a_{dd} = 131a_0$ (a_0 the Bohr radius), and it has been recently shown to have a much longer lifetime with respect to the other magnetic atoms (^{162}Dy and ^{166}Er) [9].

The eGPE admits solutions of different nature depending on ε_{dd}, which can be experimentally tuned by modifying the s-wave scattering length through Feshbach resonances. We find that for $\varepsilon_{dd} < 1.42$ the solution corresponds to a fully superfluid Bose-Einstein condensate [Fig. 1(a)], with the shape of the density profile given by an inverted parabola [46]. As ε_{dd} increases the role of the dipolar, interaction becomes more and more important and is at the origin of a rotonic structure in the excitation spectrum [47,48], observed experimentally in [49]. The softening of the roton gap eventually causes the transition to a density modulated structure: in the interval $1.42 < \varepsilon_{dd} < 1.52$, the density profile of the equilibrium configuration is characterized by typical overlapping density peaks, corresponding to the supersolid phase [see Fig. 1(b)]. For larger values of ε_{dd}, the density peaks do not overlap anymore and form an incoherent crystal of self-bound droplets [see Fig. 1(c)].

Once the phase diagram is known, we determine the moment of inertia by adding the term $-\Omega\hat{L}_z\Psi$ to Eq. (2) and evaluating the angular momentum. Since the velocity field obtained within the eGPE has the irrotational form $\mathbf{v}(\mathbf{r}) = (\hbar/m)\nabla S(\mathbf{r})$, fixed by the gradient of the phase $S(\mathbf{r})$ of the macroscopic wave function $\Psi(\mathbf{r}) = \sqrt{n(\mathbf{r})}\exp[iS(\mathbf{r})]$, this theory cannot describe a rigid rotational flow of the form $\mathbf{v} = \boldsymbol{\Omega}\wedge\mathbf{r}$. Nevertheless, if the density profile is not rotationally invariant, the moment of inertia can become large and even approach the rigid value, $\Theta_{\rm rig} = \int d\mathbf{r}(x^2+y^2)n(\mathbf{r})$, as a consequence of the mechanical drag caused by the rotation. This is the case

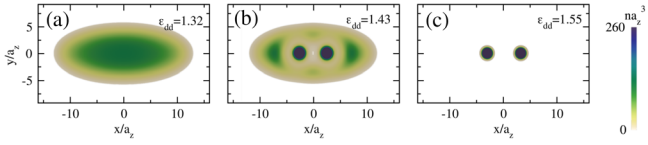

FIG. 1. Typical *in situ* density profiles obtained from the stationary solution of the eGPE (2), for different values of ε_{dd} (lengths are given in terms of the harmonic oscillator length $a_z = \sqrt{\hbar/m\omega_z} = 0.87$ μm). Three different regimes are clearly distinguishable: (a) superfluid phase (for $\varepsilon_{dd} = 1.32$), (b) supersolid phase (for $\varepsilon_{dd} = 1.43$), and (c) an incoherent *crystal* of two self-bound droplets (for $\varepsilon_{dd} = 1.55$). Notice that the color scale is saturated in (b) and (c), where the maximum value of the density reaches $na_z^3 = 900$ and 1800, respectively.

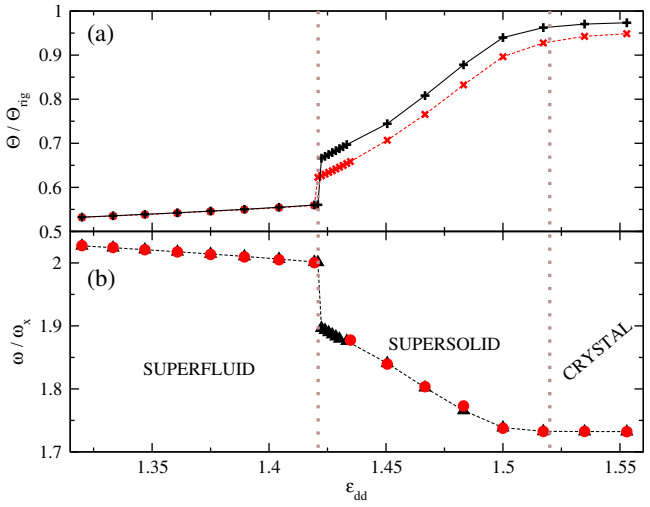

FIG. 2. (a) Moment of inertia Θ of a dipolar gas in an axially deformed harmonic trap ($\omega_y/\omega_x = 2$), as function of ε_{dd}. The black solid line shows the results of the eGPE calculations carried out with an angular momentum constraint, and the red dotted line shows the estimate given by Eq. (3). (b) Frequency of the scissor mode as function of ε_{dd}. The black dotted line corresponds to the sum rule estimate (1). Red circles correspond to the frequency of the time-dependent signal $\langle xy \rangle$ obtained from GP real-time simulations.

even in the fully superfluid phase if the trapping potential is highly elongated. It is, in fact, immediate to see that the variational result [36,50]

$$\Theta_{\mathrm{var}} = \left(\frac{\langle x^2 - y^2 \rangle}{\langle x^2 + y^2 \rangle} \right)^2 \Theta_{\mathrm{rig}} \tag{3}$$

for the moment of inertia, derivable making the ansatz $S = \alpha xy$ for the phase of the macroscopic wave function and satisfying the inequality $\Theta_{\mathrm{var}} \leq \Theta$, approaches the rigid value for highly deformed configurations corresponding to $|\langle x^2 - y^2 \rangle| \simeq \langle x^2 + y^2 \rangle$. In this extreme limit, it is not possible to reveal the effects of superfluidity through the measurement of the scissors frequency Eq. (1), and it is therefore convenient to work with moderately deformed traps. For this reason, we have chosen the value $\omega_y/\omega_x = 2$ for the in-plane aspect ratio. It is worth noticing that in the fully superfluid phase the variational result Eq. (3) coincides with the prediction of the hydrodynamic equations of superfluids [36,50]. It can be also derived miroscopically in the case of the ideal Bose gas [51].

The results of our calculations for the moment of inertia are reported in Fig. 2(a) in units of the rigid value. In the supersolid phase, the ratio $\Theta/\Theta_{\mathrm{rig}}$ significantly increases as a consequence of the presence of the density peaks which provides a solidlike contribution to Θ. The transition between the superfluid and the supersolid phase is characterized by a visible jump that reflects its first order nature [15,19,21,23,52]. By further increasing the value of ε_{dd}, the moment of inertia eventually approaches the rigid value, reflecting the crystalline nature of the self-bound droplet phase. However, even in the crystal phase, the rigid body value is not exactly achieved since each droplet is itself superfluid and cannot host a rigid rotational motion. Because of the small size of each droplet (compared to the inter droplet distance) as well as of the anisotropy of the trap, the difference between the rigid body value and the one of the crystal phase is nevertheless almost negligible. In the elongated case, reported in Fig. 2, it amounts to a few percent for the largest values of ε_{dd}. In Fig. 2, we also report (see red dotted line) the prediction of the approximate variational estimate (3), which perfectly matches the numerical result in the fully superfluid regime ($\varepsilon_{dd} < 1.43$), while for larger values of ε_{dd}, it underestimates the actual value of the moment of inertia.

The moment of inertia can be used to estimate the frequency of the scissors mode, employing Eq. (1). The predicted value ranges from the usual Bose-Einstein condensate value $\sqrt{\omega_y^2 + \omega_x^2} = 2.23\omega_x$ [30] for $\varepsilon_{dd} \to 0$, to the value $\sqrt{\omega_y^2 - \omega_x^2} = 1.73\omega_x$ in the opposite limit of large ε_{dd}, when $\langle y^2 \rangle \ll \langle x^2 \rangle$ and the moment of inertia takes the rigid value. The results for the frequency obtained within the sum rule approach are reported as black triangles in Fig. 2(b) as a function of ε_{dd}. In order to certify the validity of the sum rule prediction, we have carried out real-time simulations of the eGPE by generating initially a sudden rotation of the confining trap. The relevant signal associated with the rotation of the cloud is provided by the quantity $\langle xy \rangle$. The simulation reveals the occurrence of a single well-defined frequency for all values of ε_{dd}, which is in perfect agreement with the sum rule approach, as shown by the red dots in Fig. 2(b). Measuring the jump in the frequency of the scissors mode at the superfluid-supersolid transition would provide an important proof of its first order nature.

Nonclassical moment of inertia and quantized vortices in an isotropic trap.—If the confining potential is isotropic in the rotational plane ($\omega_x = \omega_y$), we find that, for $N = 10^5$ ^{164}Dy atoms and trapping frequencies equal to $\omega_{x,y,z} = 2\pi \times (40, 40, 80)$ Hz, the formation of the supersolid phase emerges at the value $\varepsilon_{dd} = 1.32$, with a density profile characterized by overlapping droplets arranged in triangular cells (see also [25,26]). The number and the distribution of the peaks depend on the atom number, the trapping frequencies, and the scattering length. Nevertheless, the distance between droplets is essentially the same for all the configurations considered in the present work, and agrees rather well with the value of $2\pi/q_R = 4.5a_z$ predicted in 2D uniform matter [47], where the roton wave vector q_R is determined by the axial confinement length $a_z = \sqrt{\hbar/(m\omega_z)} = 0.87$ μm.

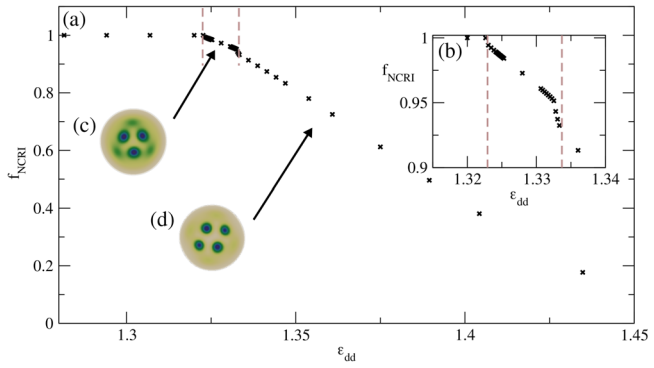

FIG. 3. (a) Nonclassical rotational inertia fraction (4) of a dipolar gas in an isotropic harmonic potential $\omega_y = \omega_x$ as a function of ε_{dd}. The brown dashed lines indicate the position of two jumps. (b) Zoom in the region $1.315 < \varepsilon_{dd} < 1.34$, where the moment of inertia presents the two jumps. (c), (d) Plot of the density in the region where the system presents a single-triangular cell and a two-triangular cell configuration, respectively.

In isotropic configurations, the moment of inertia fixes the nonclassical rotational inertia (NCRI) fraction f_{NCRI} according to the relation [53]

$$f_{\mathrm{NCRI}} = 1 - \Theta/\Theta_{\mathrm{rig}}. \tag{4}$$

In the case of a ring geometry, this quantity coincides with the superfluid fraction defined in [55,56]. In Fig. 3, we report our predictions for f_{NCRI} as a function of the dimensionless parameter ε_{dd}. This quantity exhibits a jump at the transition to the supersolid phase, which is much smaller than in the case of elongated trapping, followed by a further jump around $\varepsilon_{dd} = 1.335$, corresponding to a change of the supersolid structure from the single-triangular cell [Fig. 3(c)] to the two triangular-cell [Fig. 3(d)] configuration. For larger values of ε_{dd}, the NCRI fraction continues decreasing, the global behavior being similar to the one of the superfluid fractions calculated in periodic configurations as a function of ε_{dd}, both in the 1D [23] and in the 2D [25] cases. In order to get a better insight on the rotational effects taking place in the supersolid phase, we show in Fig. 4 the velocity field $\mathbf{v}(\mathbf{r}) = (\hbar/m)\nabla S(\mathbf{r})$ of the rotating supersolid ($\varepsilon_{dd} = 1.347$). Despite the irrotational nature of the eGPE, the figure clearly reveals the rotational motion of the droplets through the superfluid, which reacts to the motion of the droplets.

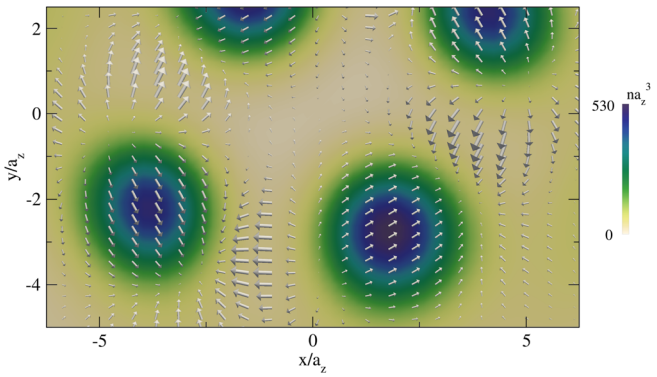

FIG. 4. Velocity field of a supersolid at small Ω. The droplets partially follow the rigid body rotation, being dragged by the $-\Omega\hat{L}_z$ term of the Hamiltonian.

The isotropic rotating configuration is very well suited to explore another important effect of superfluidity, i.e., the emergence of quantized vortices. Indeed, we find that at higher values of the angular velocity Ω, the supersolid is able to sustain a quantized vortex, thanks to the existence of an important superfluid component. In Fig. 5, we show the 2D density profiles of a rotating supersolid configuration at frequency $\Omega = 0.1\omega_x$ both in the single-triangular cell and the two-triangular cell structure cases. The presence of the vortex is clearly revealed by the vanishing of the density in the region of the vortex core (and—not shown—by the typical divergent behavior of the velocity field in the proximity of the center of the core), an effect directly measurable in future experiments. Remarkably, due to the small value of the density in the superfluid region and the vicinity of the surrounding droplets, the core of the vortex is large and deformed. The core deformation strongly depends on the structure of the droplets, being triangular-shaped and oblate in Figs. 5(b) and 5(d), respectively. We find that the vortical solution becomes the ground state configuration for $\Omega > \Omega_c \sim 0.12\omega_x$, i.e., for values of Ω significantly smaller than in the case of usual condensates [36]. The effect is the consequence of the small value of the density in the region where the vortex is formed. Furthermore, we find that the jump in the angular momentum per particle, caused by the appearance of the vortex, is

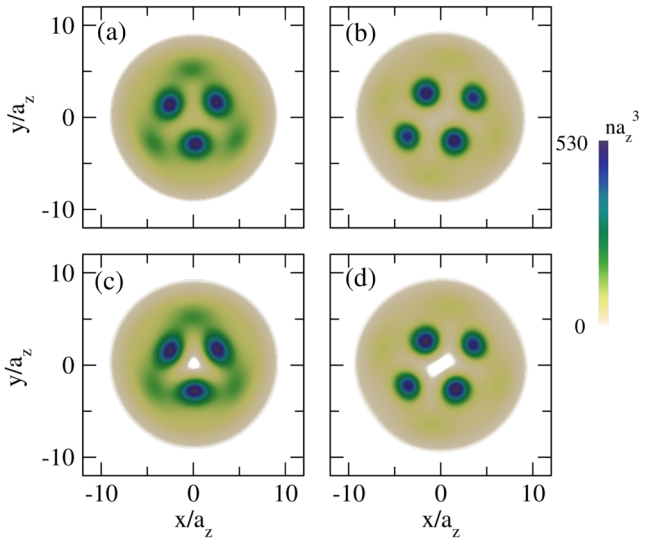

FIG. 5. Density plots of the ground state and vortical configuration: (a), (c) in the single-triangular cell structure for $\varepsilon_{dd} = 1.334$; (b),(d) in the case of a two-triangular cell structure obtained for $\varepsilon_{dd} = 1.351$.

smaller than $\hbar$, reflecting the fact that the superfluid fraction is smaller than 1 in the supersolid phase. A more systematic discussion of the behavior of vortices in the supersolid phase will be the object of a future work.

In conclusion, we have shown that supersolid dipolar atomic gases confined in harmonic traps reveal important superfluid features. In the case of elongated configurations in the plane of rotation, we have shown that the frequency of the scissors mode is a direct indicator of the effects of superfluidity on the moment of inertia, while in the case of isotropic trapping, we have shown that, remarkably, the supersolid can host a quantized vortex whose core exhibits a characteristic deformed shape, caused by the presence of the surrounding droplets. Our theoretical predictions suggest that future measurements of the rotational effects will provide new light on the superfluid behavior of these novel systems.

While completing this work, we became aware of a very recent experimental work [54] reporting the measurement of the scissors mode frequency in a dipolar supersolid and showing a very good agreement with our prediction.

Stimulating discussions with Francesca Ferlaino, Giacomo Lamporesi, Giovanni Modugno, Tilman Pfau, and Luca Tanzi are acknowledged. This project received funding from the European Union's Horizon 2020 research and innovation programme under Grant No. 641122 "QUIC", from Provincia Autonoma di Trento, the Q@TN initiative and the FIS$\hbar$ project of the Istituto Nazionale diFisica Nucleare.

*Corresponding author.
alessio.recati@ino.it

[1] E. Kim and M. H. W. Chan, Nature (London) **427**, 225 (2004).
[2] S. Balibar, Nature (London) **464**, 176 (2010).
[3] D. Y. Kim and M. H. W. Chan, Phys. Rev. Lett. **109**, 155301 (2012).
[4] J. Léonard, A. Morales, P. Zupancic, T. Esslinger, and T. Donner, Nature (London) **543**, 87 (2017).
[5] J. Léonard, A. Morales, P. Zupancic, T. Donner, and T. Esslinger, Science **358**, 1415 (2017).
[6] J.-R. Li, J. Lee, W. Huang, S. Burchesky, B. Shteynas, F. Ç. Top, A. O. Jamison, and W. Ketterle, Nature (London) **543**, 91 (2017).
[7] L. Tanzi, E. Lucioni, F. Famà, J. Catani, A. Fioretti, C. Gabbanini, R. N. Bisset, L. Santos, and G. Modugno, Phys. Rev. Lett. **122**, 130405 (2019).
[8] F. Böttcher, J.-N. Schmidt, M. Wenzel, J. Hertkorn, M. Guo, T. Langen, and T. Pfau, Phys. Rev. X **9**, 011051 (2019).
[9] L. Chomaz, D. Petter, P. Ilzhöfer, G. Natale, A. Trautmann, C. Politi, G. Durastante, R. M. W. van Bijnen, A. Patscheider, M. Sohmen *et al.*, Phys. Rev. X **9**, 021012 (2019).
[10] L. Tanzi, S. M. Roccuzzo, E. Lucioni, F. Famà, A. Fioretti, C. Gabbanini, G. Modugno, A. Recati, and S. Stringari, Nature (London) **574**, 382 (2019).
[11] M. Guo, F. Böttcher, J. Hertkorn, J.-N. Schmidt, M. Wenzel, H. P. Büchler, T. Langen, and T. Pfau, Nature (London) **574**, 386 (2019).
[12] G. Natale, R. M. W. van Bijnen, A. Patscheider, D. Petter, M. J. Mark, L. Chomaz, and F. Ferlaino, Phys. Rev. Lett. **123**, 050402 (2019).
[13] A. F. Andreev and I. M. Lifshitz, Zh. Eksp. Teor. Fiz. **56**, 2057 (1969). [Sov. Phys. JETP **29**, 1107 (1969)].
[14] W. M. Saslow, Phys. Rev. B **15**, 173 (1977).
[15] Y. Pomeau and S. Rica, Phys. Rev. Lett. **72**, 2426 (1994).
[16] D. T. Son, Phys. Rev. Lett. **94**, 175301 (2005).
[17] C.-D. Yoo and A. T. Dorsey, Phys. Rev. B **81**, 134518 (2010).
[18] C. Josserand, Y. Pomeau, and S. Rica, Phys. Rev. Lett. **98**, 195301 (2007).
[19] S. Saccani, S. Moroni, and M. Boninsegni, Phys. Rev. Lett. **108**, 175301 (2012).
[20] F. Ancilotto, M. Rossi, and F. Toigo, Phys. Rev. A **88**, 033618 (2013).
[21] T. Macrì, F. Maucher, F. Cinti, and T. Pohl, Phys. Rev. A **87**, 061602(R) (2013).
[22] G. I. Martone, Y. Li, and S. Stringari, Phys. Rev. A **90**, 041604(R) (2014).
[23] S. M. Roccuzzo and F. Ancilotto, Phys. Rev. A **99**, 041601(R) (2019).
[24] J. Hertkorn, F. Böttcher, M. Guo, J.-N. Schmidt, T. Langen, H. P. Büchler, and T. Pfau, Phys. Rev. Lett. **123**, 193002 (2019).
[25] Y.-C. Zhang, F. Maucher, and T. Pohl, Phys. Rev. Lett. **123**, 015301 (2019).
[26] Y. Kora and M. Boninsegni, J. Low Temp. Phys. **197**, 337 (2019).
[27] N. L. Iudice and F. Palumbo, Phys. Rev. Lett. **41**, 1532 (1978).
[28] E. Lipparini and S. Stringari, Phys. Lett. **130B**, 139 (1983).
[29] D. Bohle, A. Richter, W. Steffen, A. Dieperink, N. L. Iudice, F. Palumbo, and O. Scholten, Phys. Lett. **137B**, 27 (1984).
[30] D. Guéry-Odelin and S. Stringari, Phys. Rev. Lett. **83**, 4452 (1999).
[31] O. M. Maragò, S. A. Hopkins, J. Arlt, E. Hodby, G. Hechenblaikner, and C. J. Foot, Phys. Rev. Lett. **84**, 2056 (2000).
[32] A. Minguzzi and M. P. Tosi, Phys. Rev. A **63**, 023609 (2001).
[33] M. J. Wright, S. Riedl, A. Altmeyer, C. Kohstall, E. R. Sanchez Guajardo, J. H. Denschlag, and R. Grimm, Phys. Rev. Lett. **99**, 150403 (2007).
[34] C. D. Rossi, R. Dubessy, K. Merloti, M. de Goër de Herve, T. Badr, A. Perrin, L. Longchambon, and H. Perrin, New J. Phys. **18**, 062001 (2016).
[35] I. Ferrier-Barbut, M. Wenzel, F. Böttcher, T. Langen, M. Isoard, S. Stringari, and T. Pfau, Phys. Rev. Lett. **120**, 160402 (2018).
[36] L. Pitaevskii and S. Stringari, *Bose-Einstein Condensation and Superfluidity* (Oxford University Press, Oxford, 2016).
[37] F. Wächtler and L. Santos, Phys. Rev. A **93**, 061603(R) (2016).
[38] R. Schützhold, M. Uhlmann, Y. Xu, and U. R. Fischer, Int. J. Mod. Phys. B **20**, 3555 (2006).

[39] A. R. P. Lima and A. Pelster, Phys. Rev. A **86**, 063609 (2012).
[40] H. Saito, J. Phys. Soc. Jpn. **85**, 053001 (2016).
[41] D. S. Petrov, Phys. Rev. Lett. **115**, 155302 (2015).
[42] C. R. Cabrera, L. Tanzi, J. Sanz, B. Naylor, P. Thomas, P. Cheiney, and L. Tarruell, Science **359**, 301 (2018).
[43] P. Cheiney, C. R. Cabrera, J. Sanz, B. Naylor, L. Tanzi, and L. Tarruell, Phys. Rev. Lett. **120**, 135301 (2018).
[44] G. Semeghini, G. Ferioli, L. Masi, C. Mazzinghi, L. Wolswijk, F. Minardi, M. Modugno, G. Modugno, M. Inguscio, and M. Fattori, Phys. Rev. Lett. **120**, 235301 (2018).
[45] G. Ferioli, G. Semeghini, L. Masi, G. Giusti, G. Modugno, M. Inguscio, A. Gallemí, A. Recati, and M. Fattori, Phys. Rev. Lett. **122**, 090401 (2019).
[46] R. M. W. van Bijnen, N. G. Parker, S. J. J. M. F. Kokkelmans, A. M. Martin, and D. H. J. O'Dell, Phys. Rev. A **82**, 033612 (2010).
[47] L. Santos, G. V. Shlyapnikov, and M. Lewenstein, Phys. Rev. Lett. **90**, 250403 (2003).
[48] D. H. J. O'Dell, S. Giovanazzi, and G. Kurizki, Phys. Rev. Lett. **90**, 110402 (2003).
[49] L. Chomaz, R. M. W. van Bijnen, D. Petter, G. Faraoni, S. Baier, J. H. Becher, M. J. Mark, F. Wächtler, L. Santos, and F. Ferlaino, Nat. Phys. **14**, 442 (2018).
[50] A. L. Fetter, J. Low Temp. Phys. **16**, 533 (1974).
[51] S. Stringari, Phys. Rev. Lett. **76**, 1405 (1996).
[52] Z.-K. Lu, Y. Li, D. S. Petrov, and G. V. Shlyapnikov, Phys. Rev. Lett. **115**, 075303 (2015).
[53] The relationship between the moment of inertia and the NCRI fraction can be identified also in the case of anisotropic confinement in the rotational plane by using the phenomenological relation $\Theta = (1 - f_{\mathrm{NCRI}})\Theta_{\mathrm{rig}} + f_{\mathrm{NCRI}}\beta^2\Theta_{\mathrm{rig}}$, recently employed in [54], where $\beta = \langle x^2 - y^2\rangle/\langle x^2 + y^2\rangle$ is the deformation of the atomic cloud.
[54] L. Tanzi, J. G. Maloberti, G. Biagioni, A. Fioretti, C. Gabbanini, and G. Modugno, arXiv:1912.01910.
[55] A. J. Leggett, Phys. Rev. Lett. **25**, 1543 (1970).
[56] A. J. Leggett, J. Stat. Phys. **93**, 927 (1998).